Optimal Tuning of Local Voltage Control Rule of Load Tap Changers for Dynamic Operation of Unbalanced Distribution Networks

Alper Savasci*, *Member, IEEE,* Adedoyin Inaolaji , *Student Member, IEEE,* Sumit Paudyal, *Member, IEEE,*

***Abstract*—A bang-bang type control rule is typically adopted to automate the tap-changing process of on-load tap changers (OLTCs) and step voltage regulators (SVRs). The control rule is mainly characterized by a dead band parameter affecting voltage regulation performance. Due to the intermittent large-scale photovoltaic (PV) penetration, dynamic voltage fluctuations are induced along the distribution feeder, leading to frequent tap switching and equipment wear and tear. This paper proposes an optimization-based dead band tuning method to reduce the number of tap switching and lengthen the economic use-life of the regulation equipment. Unlike existing works that often ignore the local controller mechanism of tap changers, this work extends the modeling efforts by formulating the dead band tuning as a distribution system optimal power flow (DOPF) problem by considering the unbalanced characteristics of multi-phase feeders. The overall DOPF is formulated as a mixed-integer linear program (MILP) to minimize the daily total number of tap switching and the amount of curtailed energy from the PV-based inverters while maintaining voltage regulation performance. Extensive numerical tests conducted on the IEEE 13-bus and IEEE 123-bus test networks suggest that the number of tap switching can further be minimized with the use of a dynamic dead band tuning strategy.**

***Index Terms*—Distribution grid modeling, legacy device, optimal power flow, voltage regulation, mixed-integer programming**

I. Introduction

A. Background

Voltage regulation in distribution networks is conventionally carried out via utility-owned legacy devices such as on-load tap changers (OLTCs), step voltage regulators (SVRs), and fixed/switched capacitor banks (CBs) [1]. Although legacy devices are economically viable options for many utilities, they generally involve mechanical switching parts that are notorious for having limited use life. Moreover, fast mechanical degradation is likely to occur when excessive switching is executed due to the fast dynamic voltage fluctuations such as rise/fall and flickers, which is very common in photovoltaic (PV)-rich feeders [2]. In addition, reverse power flow might be coexistent due to the temporal mismatch between the PV production and consumption, which causes overvoltage and equipment overloading issues unless the proper controls are carried out [3, 4].

A. Savasci, A. Inaolaji, and S. Paudyal are with the Department of Electrical and Computer Engineering, Florida International University, Miami, USA. *Corresponding Author, Email: asava014@fiu.edu. This work is supported by the U.S. Department of Energy's Office of Energy Efficiency and Renewable Energy (EERE) under the Solar Energy Technologies Office Award Number DE-EE0008774.

In this regard, the site controllers of inverter-based resources (IBRs) and common voltage regulation devices can be coordinated through an advanced distribution management system (ADMS). In modern distribution networks, voltage regulation has been coordinated through an integrated Volt/VAR control (IVVC) as an ADMS function [5]. This framework is tightly coupled with a telemetry system, collecting measurements via strategically located sensors and sending control signals to the remote units [6]. The IVVC can directly command remote regulation devices or set their controller parameters for autonomous operation.

B. Review of Existing Literature

The majority of the existing works regarding the coordination of voltage regulation assets can be divided into two main categories:

1) Directly determining control actions by a scheme executed in a central or distributed way. Such an algorithm can periodically set the tap positions of OLTCs and SVRs (collectively referred to as LTCs), enable/disable the capacitor units residing in CBs, and dispatch the active and reactive power set points of IBRs. In this category, the local controllers are generally assumed to be either disabled or ignored.
2) Instead of computing all the control actions, the approaches in the second category let local controllers carry out their control actions with respect to the local measurements. The equipment-specific parameters associated with the local controllers are computed or tuned regularly or on-demand basis.

Distribution System Optimal Power Flow (DOPF)-based coordination schemes attract increasing interest for the first category approaches since significant advancements have been made in both hardware and software technologies in the last two decades [7, 8]. Another reason is that a DOPF solves an explicit power flow problem for the full structure of the network. Hence, the controller, i.e., DOPF, involves the model of the controlled system to some extent depending on the power flow model used [9, 10]. Due to the nonconvex and nonlinear nature of the power flow equations, finding the optimal solution of DOPF is challenging, and further complexities are added when equipment-specific controls are integrated into a DOPF formulation. In particular, the control of legacy devices via a DOPF framework inevitably introduces discrete control

variables to represent the exact discrete operations or states, thereby rendering the DOPF problem as a mixed integer nonlinear programming (MINLP) formulation.

In [11], a DOPF-based central coordination scheme has been formulated as an MINLP to be solved for a look ahead horizon to set tap positions of LTCs and the status of switched capacitors. However, the solution complexity of an MINLP is generally high and does not scale well with the number of legacy devices, making it a computationally intractable problem even for small-sized test networks. To alleviate the solution complexity, discrete variables can be relaxed into continuous variables during the solution process. Once the solution is obtained, the continuous values are then rounded to the nearest integer value [12]. However, it has been demonstrated in [13] that such rounding heuristics can lead to suboptimal and even infeasible solutions. Although the integrality constraint is removed on discrete variables, the nonconvexity may still exist in terms of continuous variables due to the power flow equations. Thus, there are two standard methods to mitigate the solution complexity: 1) relaxing the integrality and/or 2) maintaining formulation convexity. However, the latter provides stronger benefits than the former.

Convex relaxations and approximations of the original nonconvex DOPF problem can be adopted to form convex DOPF models. This is an imperative performance criterion to utilize modern mixed-integer programming solvers fully. Hence, mixed-integer convex DOPF formulations can be solved to optimally dispatch the discrete and continuous controllable assets in the distribution networks. In [13], a conic reformulation of an LTC model is combined with a second-order cone programming (SOCP) relaxation of the power flow model to yield a mixed-integer SOCP (MISOCP) formulation of DOPF that outperforms its MINLP counterpart in terms of scalability and computation time. Using the binary expansion technique, another attractive MISOCP model is proposed in [14] to optimally dispatch integer tap positions of LTCs. Similarly, in [15], an MISOCP version of DOPF is formulated to dispatch LTCs; extensive computational tests are conducted to investigate the efficiency of the proposed model under single- and multi-period operation scenarios with PV-based distributed energy resources (DERs). The authors in [12] formulated a rank-constrained semidefinite program (SDP) to set tap positions of LTCs in unbalanced networks. The formulation is solved by relaxing the nonconvex rank constraint, and then by rounding, integer tap positions are derived from voltage ratios. In [16], a two-stage scheme is proposed as a mixed-integer linear program (MILP) to optimally dispatch LTCs and CBs coordinately with smart inverters (SIs) for unbalanced networks.

Unlike the works in [12–16], other studies such as [17–20] consider the local control rules of LTCs. In this context, a strategy is proposed in [17], which coordinates the simultaneous operation of substation OLTC, feeder SVRs, and a synchronous machine-based DER unit for voltage regulation support. The proposed method uses time delay coordination and modified voltage control methods of SVRs and DER units to reduce the tap operations and the dithering effect in the feeder voltage profile. A priority-based approach has been proposed in [21] to determine the action of each device in the system based on a zone discrimination concept. Accordingly, only a sufficient set of devices should respond to any given case in the correct order to mitigate voltage fluctuations. In [18], a coordinated control scheme of substation OLTC and SIs of PV plants is devised, in which the tap position of LTC is derived hourly, based on the measured voltage at the feeder end through a remote-monitoring system. To prevent intra-hour overvoltage violations caused by PV-induced fluctuations, the outputs of SIs are sequentially controlled by changing the power factor with respect to the measured voltage. If this function does not provide sufficient voltage support to resolve the overvoltage issues, SIs start curtailing real power output based on a Volt-Watt function with hysteresis. In [19], LTC tap positions are autonomously adjusted by the bang-bang control rule, considering the load diversity. In [20], a compound optimization routine is proposed for optimizing the operation of PV-based DERs to minimize tap operations, assuming that the LTCs work autonomously based on a conventional bang-bang control rule.

C. Technical Contributions

The main contributions of this paper are as follows:

- The modeling efforts proposed in [15, 20] are extended by combining the local bang-bang controller model of common LTCs particularly for multi-phase distribution feeders with unbalanced operation. Although [15, 16] propose mathematical models for the branches with OLTC and SVRs for single- and multi-phase branch configurations, the local controller model is disregarded. The local control rule is then considered in [20] for only single-phase networks. As a further improvement, this paper generalizes and computationally evaluates the effectiveness of the local bang-bang control rule for the IEEE 13-bus and IEEE 123-bus test networks by using a multi-phase linearized DOPF model.
- The bang-bang control rule is typically characterized by the dead band parameter, which is set to a predefined value in practice based on intended voltage regulation performance. This, however, might create excessive wear and tear, leading to reliability degradation issues in DER-rich networks. Hence, in this work, we propose a scheme for tuning the dead band based on varying operating conditions caused by dynamic net loading. Similar work in [19] aims to use the dead band control; however, the optimization formulation does not consider the exact control rule. Instead, further rounding is applied to the resulting tap values, which may not always provide physically feasible tap values as shown in [13]. In contrast, this paper retains the discrete nature of the local LTC control rule and does not resort to any rounding heuristics.

The rest of this paper is organized as follows. Section II describes the mathematical models of the distribution network and major component models. Section III presents the dead band tuning approach within an optimization framework. Section IV describes the test feeder setup and discusses the results based on the case studies. Section V concludes the paper.

II. Mathematical Models

A. Distribution Network and Power Flow Model

Distribution networks can typically include multi-phase series and shunt components that form the topology of the network. The topology of distribution networks can be represented by a graph notation denoted as $\mathcal{G} = (\Omega_{\mathcal{N}}, \Omega_{\mathcal{E}})$, where $\Omega_{\mathcal{N}}$ is the set of buses and $\Omega_{\mathcal{E}}$ is the set of branches. A typical bus in a distribution network can accommodate multiple nodes where the phase terminals of series and shunt components are connected to each other. The available phases at a bus $i \in \Omega_{\mathcal{N}}$ can be collected by a bus phase set $\Omega_{\Phi}^{i} \subseteq \{a, b, c\}$. A branch in a distribution network connects two buses, indexed by an ordered tuple (i, j) which is included in the set of branches as $\Omega_{\mathcal{E}} = \{(i, j) | i, j \in \Omega_{\mathcal{N}}\}$. The network branches may have multiple phase terminals whose configuration is represented by a branch phase set $\Omega_{\Phi}^{ij} \subseteq \{a, b, c\}$. Various series and shunt feeder components such as distribution lines, OLTCs, SVRs, and CBs can be collected as a subset of either $\Omega_{\mathcal{E}}$ or $\Omega_{\mathcal{N}}$ with associated branch and bus phase sets.

The power flow model relates the branch flows with node voltages and forms the physics of the network. Since a typical distribution feeder has multi-phase couplings and operates under unbalanced loading conditions, the equations given in (1), known as *LinDist3Flow* [22], can be used to model the unbalanced nature of distribution network linearly as follows

$$p_j^{\phi,t} = \sum_{k:j\to k} P_{jk}^{\phi,t} - \sum_{i:i\to j} P_{ij}^{\phi,t}, \quad \forall j \in \Omega_{\mathcal{N}}, \forall \phi \in \Omega_{\Phi}^{j} \tag{1a}$$

$$q_j^{\phi,t} = \sum_{k:j\to k} Q_{jk}^{\phi,t} - \sum_{i:i\to j} Q_{ij}^{\phi,t}, \quad \forall j \in \Omega_{\mathcal{N}}, \forall \phi \in \Omega_{\Phi}^{j} \tag{1b}$$

$$v_i^{\phi,t} = v_j^{\phi,t} - \mathbb{H}_{ij}^{P}(\phi,\psi) P_{ij}^{\phi,t} - \mathbb{H}_{ij}^{Q}(\phi,\psi) Q_{ij}^{\phi,t}, \quad \forall (i,j) \in \Omega_{\mathcal{L}}, \forall \phi \in \Omega_{\Phi}^{ij}, \psi \in \Omega_{\Psi}^{ij} \tag{1c}$$

where (1a) and (1b) defines the active and reactive power balance at each feeder node, respectively. The complex net power injection at each node is decomposed into real and imaginary components as $p_j^{\phi,t} = p_j^{g,\phi,t} - p_j^{d,\phi,t}$ and $q_j^{\phi,t} = q_j^{g,\phi,t} - q_j^{d,\phi,t}$. The active and reactive power flows outgoing from bus j are denoted by $P_{jk}^{\phi,t}$ and $Q_{jk}^{\phi,t}$ while $P_{ij}^{\phi,t}$ and $Q_{ij}^{\phi,t}$ are the incoming active and reactive power flows at bus j on phase ϕ during time t. The voltage drop equation, (1c), relates the branch active $(P_{ij}^{\phi,t})$ and reactive $(Q_{ij}^{\phi,t})$ power flows with the magnitude-squared node voltages $(v_i^{\phi,t} = |\widetilde{V}_i^{\phi,t}|^2)$ by considering the multi-phase line configuration given by matrices $\mathbb{H}_{ij}^{P}$ and $\mathbb{H}_{ij}^{Q}$ as follows

$$\mathbb{H}_{ij}^{P} = \begin{bmatrix} -2r_{ij}^{aa} & r_{ij}^{ab} - \sqrt{3}x_{ij}^{ab} & r_{ij}^{ac} + \sqrt{3}x_{ij}^{ac} \\ r_{ij}^{ba} + \sqrt{3}x_{ij}^{ba} & -2r_{ij}^{bb} & r_{ij}^{bc} - \sqrt{3}x_{ij}^{bc} \\ r_{ij}^{ca} - \sqrt{3}x_{ij}^{ca} & r_{ij}^{cb} + \sqrt{3}x_{ij}^{cb} & -2r_{ij}^{cc} \end{bmatrix} \tag{1d}$$

$$\mathbb{H}_{ij}^{Q} = \begin{bmatrix} -2x_{ij}^{aa} & x_{ij}^{ab} + \sqrt{3}r_{ij}^{ab} & x_{ij}^{ac} - \sqrt{3}r_{ij}^{ac} \\ x_{ij}^{ba} - \sqrt{3}r_{ij}^{ba} & -2x_{ij}^{bb} & x_{ij}^{bc} + \sqrt{3}r_{ij}^{bc} \\ x_{ij}^{ca} + \sqrt{3}r_{ij}^{ca} & x_{ij}^{cb} - \sqrt{3}r_{ij}^{cb} & -2x_{ij}^{cc} \end{bmatrix} \tag{1e}$$

where r_{ij} and x_{ij} are resistance and reactance values which are obtained by the impedance matrix of the corresponding line configuration.

B. Modeling of LTC Branch

The OLTCs and SVRs are autotransformers that adjust a voltage difference between terminals with respect to the turns-ratio of the selected tap position. Let $\Omega_{\mathcal{H}} \subseteq \Omega_{\mathcal{E}}$ be the set of all LTC equipped branches in the network. The voltage relation between the terminals of an LTC branch can be modeled as follows

$$v_j^{\phi,t} = (1 + \delta V \cdot T_{ij}^{\phi,t})^2 v_i^{\phi,t}, \quad \forall (i,j) \in \Omega_{\mathcal{H}}, \forall \phi \in \Omega_{\Phi}^{ij} \tag{2a}$$

where $T_{ij}^{\phi,t}$ is the LTC tap position which is an integer number bounded within the range of $\pm T_{ij}^{\max}$ in practice, and δV is the step voltage change per tap. Due to bilinear and quadratic terms, 2a is a nonlinear equation. Using the binary expansion technique given in [14, 15], the integer tap values can be represented as a weighted-sum of binary digits as follows

$$T_{ij}^{\phi,t} = \sum_{n=0}^{K_{ij}^{\phi}} 2^n b_{ij,n}^{\phi,t} - T_{ij}^{\max} \tag{2b}$$

where K_{ij}^{ϕ} is the index of the most significant digit, $b_{ij,n}^{\phi,t}$ represents the corresponding binary digits. To be able to represent the negative tap values, an offset value of $T_{ij}^{\max}$ is subtracted from the first summand. Then, defining a new variable $\mu_{ij}^{\phi,t} := (1 + \delta V \cdot T_{ij}^{\phi,t}) v_i^{\phi,t}$ and using (2b), the following expanded expression can be obtained as

$$\mu_{ij}^{\phi,t} := v_i^{\phi,t} + \delta V \sum_{n=0}^{K_{ij}^{\phi}} 2^n w_{ij,n}^{\phi,t} - \delta V T_{ij}^{\max} v_i^{\phi,t} \tag{2c}$$

where $w_{ij,n}^{\phi,t} := b_{ij,n}^{\phi,t} v_i^{\phi,t}$ is defined as a semi-continuous variable that can be linearly reformulated by adding the following two inequalities as

$$0 \le w_{ij,n}^{\phi,t} \le b_{ij,n}^{\phi,t} \, \mathrm{M}_1 \tag{2d}$$

$$0 \le v_i^{\phi,t} - w_{ij,n}^{\phi,t} \le (1 - b_{ij,n}^{\phi,t}) \, \mathrm{M}_1. \tag{2e}$$

where M_1 is a sufficiently big number, which can be selected based on the operating upper bound of $v_i^{\phi,t}$. Then, 2a can be rewritten multiplying $(1 + \delta V \cdot T_{ij}^{\phi,t})$ by $\mu_{ij}^{\phi,t}$ as follows

$$\begin{aligned} v_j^{\phi,t} &= (1 + \delta V \cdot T_{ij}^{\phi,t}) \mu_{ij}^{\phi,t} \\ &= \mu_{ij}^{\phi,t} + \delta V \cdot \sum_{n=0}^{K_{ij}^{\phi}} 2^n b_{ij,n}^{\phi,t} \mu_{ij}^{\phi,t} - \delta V T_{ij}^{\max} \mu_{ij}^{\phi,t} \end{aligned} \tag{2f}$$

where the bilinear product can be eliminated by introducing a new variable $y_{ij,n}^{\phi,t} := b_{ij,n}^{\phi,t} \mu_{ij}^{\phi,t}$ and adding the associated constraints as follows

$$0 \le y_{ij,n}^{\phi,t} \le b_{ij,n}^{\phi,t} \, \mathrm{M}_2 \tag{2g}$$

$$0 \le \mu_{ij}^{\phi,t} - y_{ij,n}^{\phi,t} \le (1 - b_{ij,n}^{\phi,t}) \, \mathrm{M}_2 \tag{2h}$$

where the proper value of M_2 can be set by considering the largest possible value of $\mu_{ij}^{\phi,t}$.

$$v_j^{\phi,t} = \mu_{ij}^{\phi,t} + \delta V \cdot \sum_{n=0}^{K_{ij}^{\phi}} 2^n y_{ij,n}^{\phi,t} - \delta V T_{ij}^{\max} \mu_{ij}^{\phi,t} \tag{2i}$$

In conclusion, an LTC branch can be modeled by the constraints

$$(2b)-(2e), (2g)-(2i), \quad \forall (i,j) \in \Omega_{\mathcal{H}}, \forall \phi \in \Omega_{\Phi}^{ij}. \tag{2j}$$

C. A Bang-bang Controller Model of an LTC

The turns ratio of an LTC can be lowered or raised with respect to the measured voltage at a regulation point. Fig. 1 illustrates a conceptual block diagram of a closed-loop voltage regulation with a load tap changer (LTC) mechanism which executes the automatic tap operations based on the bang-bang control rule.

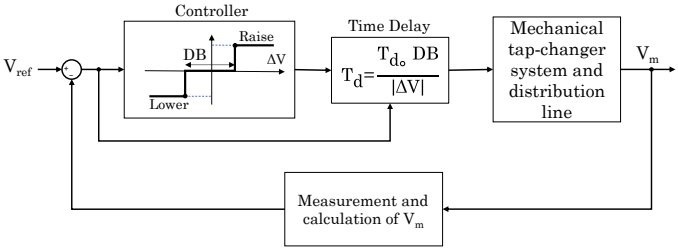

Fig. 1: Closed-loop control of an LTC [23].

In this scheme, a measured or estimated voltage V_{m} is obtained at a regulation point in the feeder and fed back to a bang-bang controller. According to the error signal, that is, the voltage difference between the reference voltage V_{ref} and V_{m}, the bang-bang controller initiates the raise or lower control actions. A typical bang-bang control rule is illustrated in Fig. 2. Depending on the calculated voltage difference, the controller initiates either raise or lower command or idle within the deadband (DB) region.

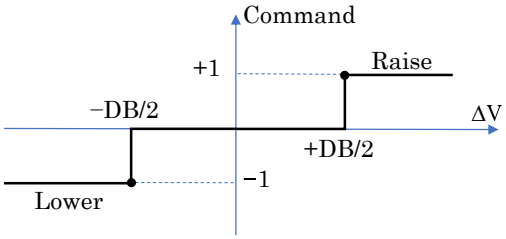

Fig. 2: Bang-bang control rule [20].

The characterizing parameter of a bang-bang control rule is the dead band (DB) that defines the range where the controller is in idle mode, i.e., neither raise nor lower action is initiated. The dead band parameter is crucial for the stable operation of the given closed-loop system [23]. Moreover, the dead band should be set based on the criteria $\mathrm{DB} > 2 \cdot \delta V$ [24]. Note that a time delay block is also appended to the controller to eliminate the unwanted frequent switching actions caused by fast voltage transients. In practice, different delay functions such as inverse, linear or conditional delay are commonly used. However, all type of delay functions use DB and a default delay coefficient (e.g. $\mathrm{T_{d_\circ}}$) and calculate the delay duration proportional to the magnitude of the voltage deviation between the reference and measured voltage at a node as follows

$$\Delta V_{ij}^{\phi,t} = V_{\mathrm{ref},ij}^{\phi,t} - V_{m_{ij}}^{\phi,t}, \quad m_{ij} \in \Omega_{\mathcal{N}}. \tag{3a}$$

where $V_{m_{ij}}^{\phi,t}$ is the node voltage sensed at bus m_{ij}. The mathematical model of the control rule (logic) can also be formulated as a mixed-integer linear form by adopting the big-M approach ($M > 0$ is a sufficiently big number). The three possible control actions can be represented by binary variables, $c_{r,ij}^{\phi,t}, c_{\ell,ij}^{\phi,t}, c_{d,ij}^{\phi,t} \in \{0,1\}$, which correspond to raise, lower and deadband, respectively. The controller only selects exactly one control action, which is enforced by the following equality constraint

$$c_{r,ij}^{\phi,t} + c_{\ell,ij}^{\phi,t} + c_{d,ij}^{\phi,t} = 1. \tag{3b}$$

The comparisons of the calculated voltage difference, ΔV, with threshold values, $-$DB/2 and $+$DB/2, of the control rule triggers either raise or lower command as follows

$$\Delta V_{ij}^{\phi,t} - (\mathrm{DB}/2) \leq c_{r,ij}^{\phi,t} \cdot \mathrm{M}_3 \tag{3c}$$

$$-\Delta V_{ij}^{\phi,t} - (\mathrm{DB}/2) \leq c_{\ell,ij}^{\phi,t} \cdot \mathrm{M}_3 \tag{3d}$$

where the fact that the $\Delta V_{ij}^{\phi,t}$ is greater than DB/2 forces the $c_{r,ij}^{\phi,t}$ to be ON since the left-hand side of (3c) becomes positive, thereby triggering the raise command. Similarly, when $\Delta V_{ij}^{\phi,t}$ is smaller than $-$DB/2, the left-hand side of (3d) becomes positive, which triggers $c_{\ell,ij}^{\phi,t}$ to be ON and the controller generates a lower command. Apart from the cases where the controller selects raise or lower command, there might be a case where $\Delta V_{ij}^{\phi,t}$ falls within the deadband, which makes the controller idle. During the idle case, $\Delta V_{ij}^{\phi,t}$ is less than DB/2 and greater than $-$DB/2, represented by the following inequalities

$$\Delta V_{ij}^{\phi,t} + (\mathrm{DB}/2) \leq d_{1,ij}^{\phi,t} \cdot \mathrm{M}_3 \tag{3e}$$

$$-\Delta V_{ij}^{\phi,t} + (\mathrm{DB}/2) \leq d_{2,ij}^{\phi,t} \cdot \mathrm{M}_3 \tag{3f}$$

where the auxiliary variables $d_{1,ij}^{\phi,t}$ and $d_{2,ij}^{\phi,t}$ are used to indicate both conditions. It is imperative that $\mathrm{M}_3 > \mathrm{DB}$. The simultaneous occurrence of both conditions is checked by coupling the auxiliary variables and $c_{d,ij}^{\phi,t}$ variables by the logical AND operator as follows

$$\left.\begin{aligned} c_{d,ij}^{\phi,t} \leq d_{1,ij}^{\phi,t}, \quad c_{d,ij}^{\phi,t} \leq d_{2,ij}^{\phi,t} \\ c_{d,ij}^{\phi,t} \geq d_{1,ij}^{\phi,t} + d_{2,ij}^{\phi,t} - 1. \end{aligned}\right\} \tag{3g}$$

Since an LTC has a limited number of tap positions, there might be extreme cases in which the tap change might be saturated in lower or raise directions. When the controller is saturated, the effect of raise or lower commanding is blocked and the tap position stays at the maximum or minimum tap position based on the previous tap value. To model the saturation properly, the conditions that trigger the raise and lower commands should be considered separately. Let $z_{1,ij}^{\phi}$ and $z_{2,ij}^{\phi}$ be auxiliary binary variables ($\in \{0,1\}$) which are used to indicate the saturation in raise direction as follows

$$T_{ij}^{\phi,t-1} - (T_{ij}^{\max} - 1) \leq z_{1,ij}^{\phi,t} \cdot \mathrm{M}_4 \tag{3h}$$

where $z_{1,ij}^{\phi}$ becomes 1 when the previous tap position hits to the maximum tap value $T_{ij}^{\max}$. However, when the previous tap

position is not $T_{ij}^{\max}$, $z_{1,ij}^{\phi}$ has to be forced to 0. This can be done by the use of $z_{2,ij}^{\phi,t}$ in the following inequality

$$T_{ij}^{\max} - T_{ij}^{\phi,t-1} \leq z_{2,ij}^{\phi,t} \cdot \mathrm{M}_4 \tag{3i}$$

where $z_{2,ij}^{\phi}$ becomes 1 when the previous tap position is different than $T_{ij}^{\max}$. Hence, $z_{1,ij}^{\phi}$ is forced to be 0 by the following equality

$$z_{1,ij}^{\phi,t} + z_{2,ij}^{\phi,t} = 1. \tag{3j}$$

Generally, LTC controller have negative tap positions in lower direction, to represent the saturation in lower direction, the following inequality can be added

$$-T_{ij}^{\phi,t-1} - (T_{ij}^{\max} - 1) \leq z_{3,ij}^{\phi,t} \cdot \mathrm{M}_4 \tag{3k}$$

where $z_{3,ij}^{\phi,t}$ becomes 1 when the previous tap position hits at lower bound. Similar to the case with raise saturation, another auxiliary variable $z_{4,ij}^{\phi,t}$ is used to represent the case where the tap position is not minimum tap value, i.e. $(-T_{ij}^{\max})$, as follows

$$T_{ij}^{\max} + T_{ij}^{\phi,t-1} \leq z_{4,ij}^{\phi,t} \cdot \mathrm{M}_4 \tag{3l}$$

where $\mathrm{M}_4 \geq 2 \cdot T_{ij}^{\max} + 1$. To force the $z_{3,ij}^{\phi,t}$ to 0, the following equality is added as

$$z_{3,ij}^{\phi,t} + z_{4,ij}^{\phi,t} = 1. \tag{3m}$$

Then, the temporal tap change process can be formulated by considering the variables $z_{1,ij}^{\phi,t}$ and $z_{3,ij}^{\phi,t}$ as follows

$$T_{ij}^{\phi,t} = T_{ij}^{\phi,t-1} + c_{r,ij}^{\phi,t}(1 - z_{1,ij}^{\phi,t}) - c_{l,ij}^{\phi,t}(1 - z_{3,ij}^{\phi,t}) \tag{3n}$$

where the effect of tap raising or lowering commands can be disabled in saturation. However, (3n) is a nonlinear equation due to the second and third summands. By reformulation techniques a linearized expression can be obtained as follows

$$\begin{aligned} T_{ij}^{\phi,t} &= T_{ij}^{\phi,t-1} + (c_{r,ij}^{\phi,t} - c_{r,ij}^{\phi,t} z_{1,ij}^{\phi,t}) - (c_{l,ij}^{\phi,t} - c_{l,ij}^{\phi,t} z_{3,ij}^{\phi,t}) \\ &= T_{ij}^{\phi,t-1} + (c_{r,ij}^{\phi,t} - z_{r,ij}^{\phi,t}) - (c_{l,ij}^{\phi,t} - z_{l,ij}^{\phi,t}) \end{aligned} \tag{3o}$$

where $z_{r,ij}^{\phi,t} := c_{r,ij}^{\phi,t} z_{1,ij}^{\phi,t}$ and $z_{l,ij}^{\phi,t} := c_{l,ij}^{\phi,t} z_{3,ij}^{\phi,t}$ which can be reformulated by using the following set of inequalities

$$\left.\begin{aligned} z_{r,ij}^{\phi,t} &\leq c_{r,ij}^{\phi,t}, \quad z_{r,ij}^{\phi,t} \leq z_{1,ij}^{\phi,t} \\ z_{r,ij}^{\phi,t} &\geq c_{r,ij}^{\phi,t} + z_{1,ij}^{\phi,t} - 1 \end{aligned}\right\} \tag{3p}$$

$$\left.\begin{aligned} z_{l,ij}^{\phi,t} &\leq c_{l,ij}^{\phi,t}, \quad z_{l,ij}^{\phi,t} \leq z_{3,ij}^{\phi,t} \\ z_{l,ij}^{\phi,t} &\geq c_{l,ij}^{\phi,t} + z_{3,ij}^{\phi,t} - 1. \end{aligned}\right\} \tag{3q}$$

Due to *LinDist3Flow* model is formulated based on the magnitude-squared voltage, v, it is compulsory to use an approximation method to couple the first-order voltage magnitude, V. Approximation with Taylor series expansion has been found as an efficient approximation in [25] as follows

$$v_{m_{ij}}^{\phi,t} \equiv (V_o^{\phi,t})^2 + 2 \cdot V_o^{\phi,t}(V_{m_{ij}}^{\phi,t} - V_o^{\phi,t}), \quad m_{ij} \in \Omega_{\mathcal{N}} \tag{3r}$$

where $V_o^{\phi,t}$ denotes the voltage at the operating point used for Taylor expansion. An LTC bang-bang controller can be modeled by the following constraints

$$(3a) - (3r), \quad \forall (i,j) \in \Omega_{\mathcal{H}}, \forall \phi \in \Omega_{\Phi}^{ij}. \tag{3s}$$

D. Operational Model of an IBR

The operational mathematical model of a PV-based IBR unit can be represented based on the capability curve illustrated in Fig. 3

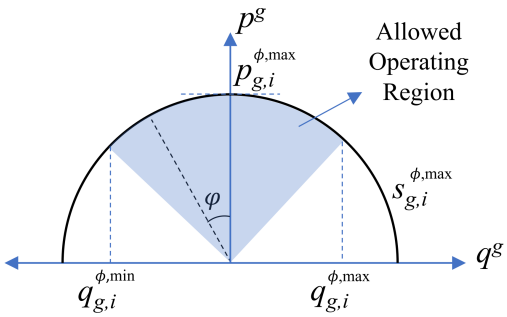

Fig. 3: Capability curve of a distributed generator [20].

Typically, the allowed operating region can be represented by a set of constraints as follows

$$p_{g,i}^{\phi,t} = p_{\mathrm{PV},i}^{\phi,t} - p_{\mathrm{curt},i}^{\phi,t} \tag{4a}$$

$$0 \leq p_{\mathrm{curt},i}^{\phi,t} \leq p_{g,i}^{\phi,\max} \tag{4b}$$

$$q_{g,i}^{\phi,\min} \leq q_{g,i}^{\phi,t} \leq q_{g,i}^{\phi,\max} \tag{4c}$$

$$-tan(\varphi_{min})\, p_{g,i}^{\phi,t} \leq q_{g,i}^{\phi,t} \leq p_{g,i}^{\phi,t}\, tan(\varphi_{max}) \tag{4d}$$

$$(p_{g,i}^{\phi,t})^2 + (q_{g,i}^{\phi,t})^2 \leq (s_{g,i}^{\phi,\max})^2 \tag{4e}$$

where $p_{\mathrm{PV},i}^{\phi,t}$ is the produced PV power by the PV system, $p_{\mathrm{curt},i}^{\phi,t}$ is the curtailed power by the PV inverter, $p_{g,i}^{\phi,t}$ and $q_{g,i}^{\phi,t}$ active and reactive power outputs, respectively. The nameplate apparent power limit of the generating unit is denoted by $s_{g,i}^{\phi,\max}$. The power outputs can be adjusted within the allowed operating region or based on a specified power factor angle (φ). The quadratic inequality (4e) can further be approximated linearly, based on [26], by making use of a 32-vertex polygon (k = 16) and defining a polyhedral norm as

$$-s_{g,i}^{\phi,\max} \leq \cos(h\gamma)\; p_{g,i}^{\phi,t} + \sin(h\gamma)\; q_{g,i}^{\phi,t} \leq s_{g,i}^{\phi,\max} \tag{4f}$$
$$\gamma = \frac{\pi}{k}, \quad h = 1, \ldots, k.$$

In distribution network, the IBR units can be collected by the set $\Omega_{\mathcal{I}} = \{i | i \in \Omega_{\mathcal{N}}\}$ with a corresponding phase set Ω_{Φ}^{i}. The operational model of an PV-based IBR unit can be modelled by the affine set of constraints as follows

$$(4a) - (4d), (4f), \quad \forall i \in \Omega_{\mathcal{I}}, \forall \phi \in \Omega_{\Phi}^{i}. \tag{4g}$$

III. Proposed Approach

A. Dead Band Tuning Process of an LTC Controller

The dead band parameter of an LTC controller can be dynamically adjusted in a way to reduce the number of daily tap operations to optimize the equipment economic life. Fig. 4 illustrates a dead band parameter adjustment concept where the break points can vary within the corresponding shaded regions by tuning dynamically.

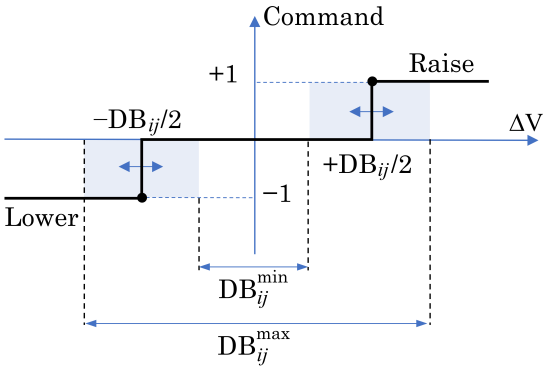

Fig. 4: LTC controller dead band adjustment.

Conventionally, the dead band parameter of an LTC controller, DB_{ij}^{t}, is set to a constant value within the range of $[\mathrm{DB}_{ij}^{\min}, \mathrm{DB}_{ij}^{\max}]$ considering the regulation feasibility and intended voltage regulation performance. Then, the following bounding relationship can formally define the dead band tuning range as follows

$$\left.\begin{aligned} 2\cdot\delta V < \mathrm{DB}_{ij}^{\phi,\min} \le \mathrm{DB}_{ij}^{\phi,t} \\ \mathrm{DB}_{ij}^{\phi,t} \le \mathrm{DB}_{ij}^{\phi,\max} \le 8\cdot\delta V \end{aligned}\right\}, \forall (i,j)\in\Omega_{\mathcal{H}},\ \forall\phi\in\Omega_{\Phi}^{ij} \quad (5a)$$

where the limits are often represented by 120 volt base [1, 24]. Accordingly, the dead band is allowed to take up to $8\cdot\delta V$ that corresponds to 6 V for 120 V base for satisfactory voltage regulation [27]. When $\mathrm{DB}_{ij}^{\phi,\min}$ and $\mathrm{DB}_{ij}^{\phi,\max}$ are set to same constant value the dead band is fixed otherwise it is allowed to vary within the specified limits.

B. A DOPF Model for Optimal Dead Band Tuning

The operational model of a distribution network can be considered as a quasi-static process within a finite-duration of time interval, t, in which all the state and control variables as well as the network parameters can be assumed as constant. Then, a daily operation horizon can be divided into multiple time intervals collected by the set of time indices, $\Omega_{\mathcal{T}} = \{1, 2, \ldots, |\Omega_{\mathcal{T}}|\}$.

The controllable equipment in the system can be dispatched periodically by solving a DOPF problem, which has been formulated to optimize a certain objective function. In this study, we propose a DOPF formulation given compactly in (6) as follows

$$\underset{p_{curt,i}^{\phi,t},\, T_{ij}^{\phi,t},\, \mathrm{DB}_{ij}^{\phi,t}}{\operatorname{argmin}} \quad J \quad (6a)$$

Subject to :

Power balance : (1a) − (1b),	$\forall t\in\Omega_{\mathcal{T}}$	(6b)
Voltage drop : (1c),	$\forall t\in\Omega_{\mathcal{T}}$	(6c)
LTC branch model : (2b) − (2e), (2g) − (2i),	$\forall t\in\Omega_{\mathcal{T}}$	(6d)
LTC cont. model : (3a) − (3r), (5a),	$\forall t\in\Omega_{\mathcal{T}}$	(6e)
IBR model : (4b) − (4d), (4f),	$\forall t\in\Omega_{\mathcal{T}}$	(6f)
Absolute Value Function : (6j)	$\forall t\in\Omega_{\mathcal{T}}$	(6g)
Upper & Lower Bounds on Variables	$\forall t\in\Omega_{\mathcal{T}}$	(6h)

with an objective function given as follows

$$\begin{aligned} J = c_1 \sum_{t\in\Omega_{\mathcal{T}}}\sum_{i\in\Omega_{\mathcal{I}}}\sum_{\phi\in\Omega_{\Phi}^{i}} p_{curt,i}^{\phi,t} \\ + c_2 \sum_{t\in\Omega_{\mathcal{T}}}\sum_{(i,j)\in\Omega_{\mathcal{H}}}\sum_{\phi\in\Omega_{\Phi}^{ij}} |T_{ij}^{\phi,t} - T_{ij}^{\phi,t-1}| \\ + c_3 \sum_{t\in\Omega_{\mathcal{T}}}\sum_{(i,j)\in\Omega_{\mathcal{H}}}\sum_{\phi\in\Omega_{\Phi}^{ij}} \mathrm{DB}_{ij}^{\phi,t} \end{aligned} \quad (6i)$$

where the first term in J is the total curtailed energy from the PV generation, the second term is the total absolute tap position change of LTCs between consecutive time intervals. The third term is the total amount of dead band of LTC controllers. The absolute value function $|\cdot|$ is nonlinear, preventing the use of efficient MILP solvers. Fortunately, it can be reformulated linearly by replacing the absolute difference with a new variable as $\xi_{ij}^{\phi,t} := |T_{ij}^{\phi,t} - T_{ij}^{\phi,t-1}|$, and then adding the following inequalities to the overall formulation (6) as

$$\left.\begin{aligned} \xi_{ij}^{\phi,t} \le T_{ij}^{\phi,t} - T_{ij}^{\phi,t-1} \\ \xi_{ij}^{\phi,t} \le T_{ij}^{\phi,t-1} - T_{ij}^{\phi,t} \end{aligned}\right\}, \forall (i,j)\in\Omega_{\mathcal{H}},\ \forall\phi\in\Omega_{\Phi}^{ij}. \quad (6j)$$

The overall OPF can be solved by properly selecting the coefficients c_1,c_2 and c_3 denoting the weights on the individual objective terms. Consequently, the overall problem is formulated as an MILP, which is a format amenable to the most common commercial and open-source optimization solvers.

IV. Numerical Results

The computational performance of the proposed approach is tested on the IEEE 13-bus and 123-bus feeders [28] with some modifications. The same base loading is used exactly given as in the IEEE test feeder data sheets by only converting all the load types into the constant-PQ type. Fig. 5 shows the normalized demand and PV generation profiles used to scale the base loading for daily operation horizon. A desktop PC with Intel(R) Core(TM) i7-10700 CPU @ 2.90 GHz was used when conducting simulations studies.

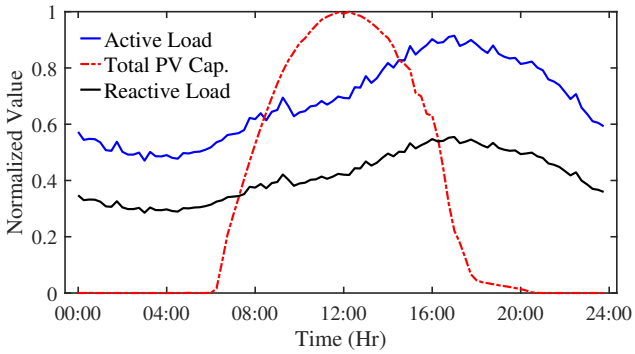

Fig. 5: Demand and PV generation capacity profiles.

A. Numerical Tests on IEEE 13-bus Feeder

The IEEE 13-bus test feeder has 1 voltage regulator located at the feeder head. The existing network has been modified by adding 2 utility-scale PV generation sites, illustrated in Fig. 6. The PV generation sites are interconnected to the network

through the three-phase inverters with a rating of 2 MVA that can be managed by the network operator directly.

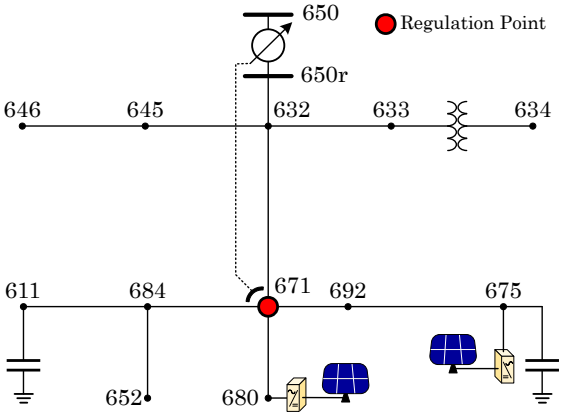

Fig. 6: The modified IEEE 13-bus test network.

In this test network, the secondary bus of the feeder regulator, labeled as $650r$, is the regulating bus in which the voltage is allowed to vary within the range of $[0.9, 1.1]$ per unit (p.u.) voltage to be able to utilize the full range of tap positions within $[-16, +16]$ with $\delta V = 0.00625$ p.u. step voltage change. The bus labeled 671 is indicated as the regulation point where the voltage is regulated by sensing the voltage deviations and executing the automatic tap position change accordingly to maintain the voltage level around the reference set point, which is often set to 1 p.u. The coefficients in (6i) is selected as $c_1 = 1000$, $c_2 = 1$, $c_3 = 100$.

Table I summarizes the total tap change count that occurred in a daily operation by using the fixed and variable dead band settings under common power factor(PF) control modalities of IBR units. The tightest bandwidth that can be set has been found as $6\delta V$ for the entire operation horizon for the considered loading and PV generation capacity, meaning that the bandwidth below $6\delta V$ does not result in a feasible solution for the entire multi-period optimization for 96 intervals with 15 minute resolution. Hence, the dead band parameter is tested for larger values by gradually increasing up to $8\delta V$ or 6 volts on 120 base voltage, which is a practical upper bound value generally set in the typical OLTC and SVR controller settings.

TABLE I: Number of Total Tap Change

Dead Band / PF Control	Fixed			Variable	
	$6\delta V$	$7\delta V$	$8\delta V$	$[6-8]\delta V$	Avg. DB
PF = 1	9	6	4	5	6.06
PF = 0.95 (lagging)	29	21	16	25	6.10
PF = 0.95 (leading)	6	3	2	4	6.03
PF $\leq$ |0.95|	14	7	1	12	6.001

It can be concluded from the average of dead band values in Table I that the dead band tuning approach is effective in approximating the tightest voltage regulation bandwidth of $6\delta V$ while achieving less number of total tap position changes compared to the fixed dead band version with $6\delta V$ over all the PF control cases. When the dead band parameter is set to a larger value, i.e., $> 6\delta V$, the total number of tap changes is reduced for all inverter control modes since the larger voltage fluctuation does not trigger additional tap raise or lower actions.

Among the PF control modalities, the lagging power factor of 0.95 incurs the highest tap position change since the PV inverter units inject capacitive reactive power in addition to the injection of the fixed capacitors in the IEEE 13-bus system. However, when the dead band tuning is used, $6.1\delta V$ average bandwidth can be maintained, resulting in a reduction of total tap changes than that of the fixed dead band counterpart as shown in Fig. 7.

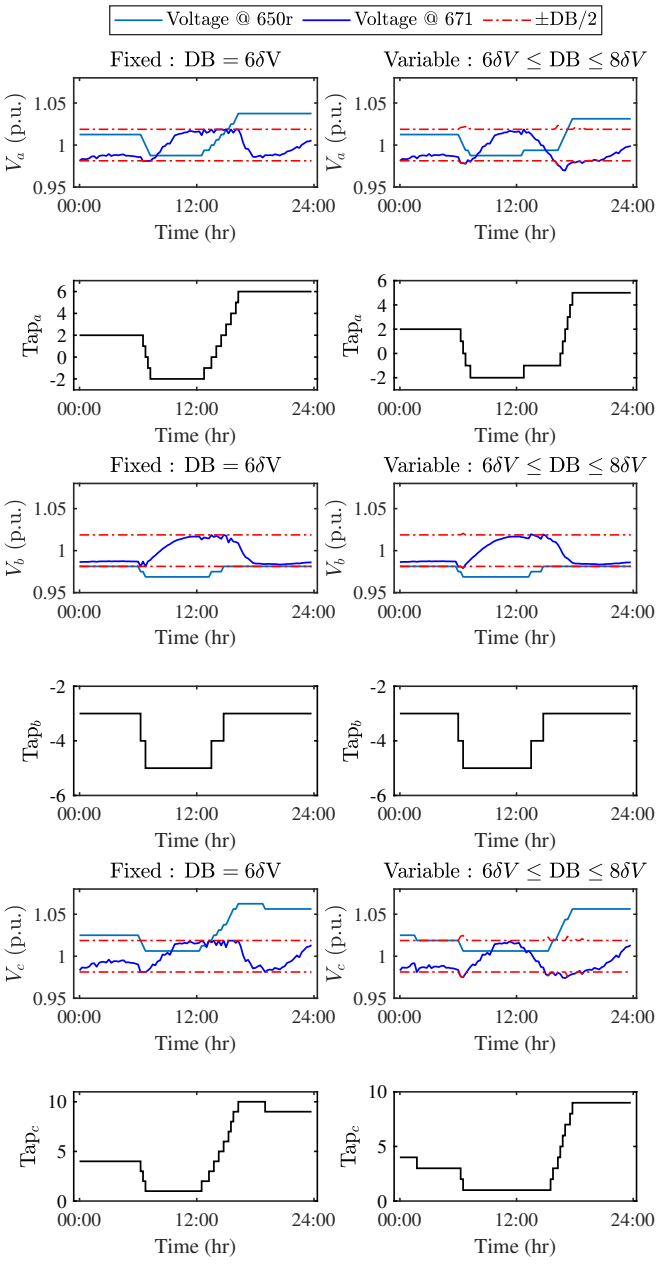

Fig. 7: Tap variations with control mode PF = 0.95 lagging.

The leading power factor of 0.95 achieves the least number of tap changes with the tightest voltage regulation bandwidth of $6\delta V$ since the reactive power is absorbed by PV inverters, which prevents the excessive voltage rise during the periods with strong irradiation as shown in Fig. 8. It can also be observed that there is a multi-phase coupling effect on the

phase voltages at the regulation point as phase-a and phase-c are in phase, whereas the voltage at phase-b is out of phase with the other phases. The dead band tuning approach reduces the total tap change of the regulator placed on phase-c at the required intervals.

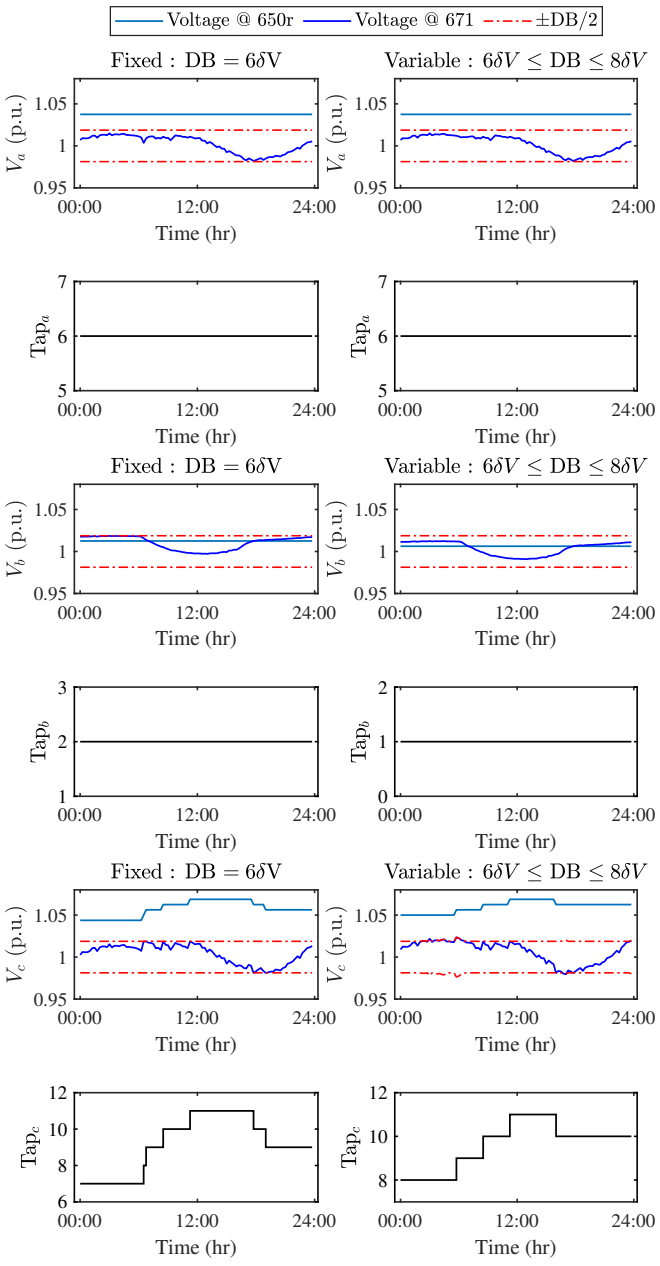

Fig. 8: Tap variations with control mode PF = 0.95 leading.

The flexible power factor control combined with the dead band tuning results in the least average bandwidth of $6.001\delta V$ while 12 tap change is initiated compared to the fixed dead band of $6\delta V$. Moreover, the flexible power factor operation significantly eliminates further tap switching with larger dead band values. Fig. 9 shows that the phase voltages at the regulation point have frequent fluctuations mainly confined within the controller dead band. When combined with this power factor control mode, the frequency of tuning actions is significantly reduced.

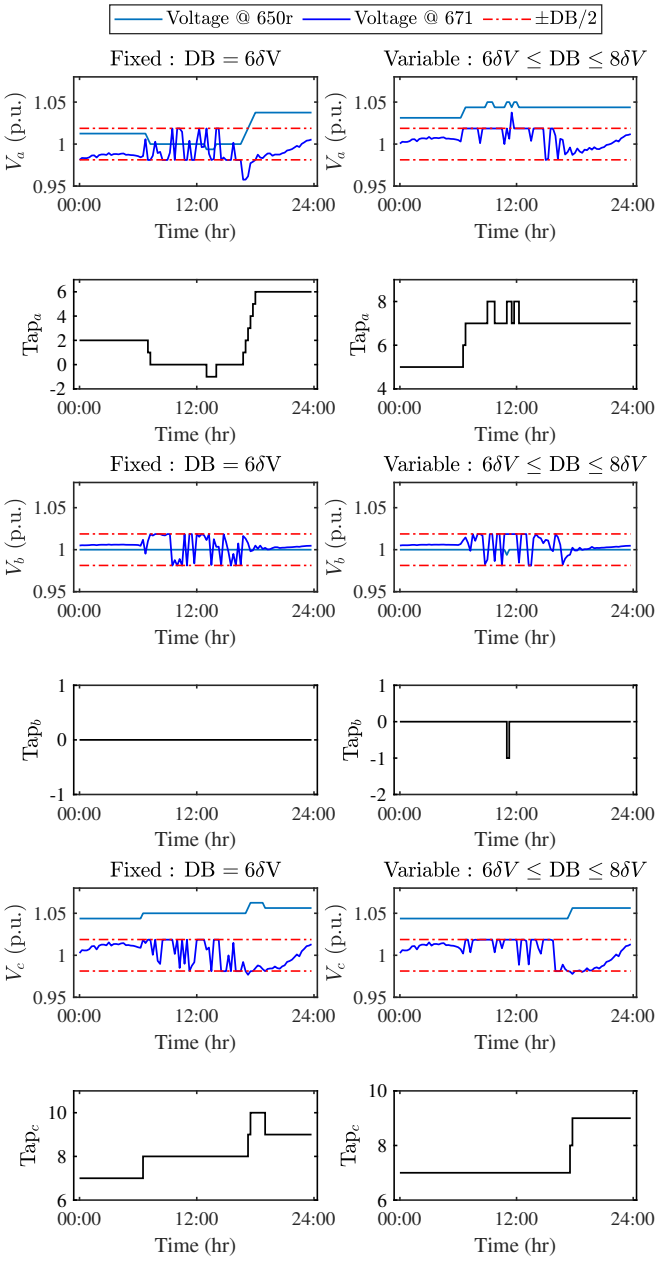

Fig. 9: Tap variations with control mode PF $\leq |0.95|$.

Table II shows the resulting total amount of curtailed energy. It can be concluded that the dead band tuning method does not curtail inverter output larger than that of the fixed dead band for all control options. When the dead band is increased from $6\delta V$ to $8\delta V$, the amount of curtailed energy is reduced in the cases with PF $= 1$ and PF $= 0.95$ lagging, even though the rate of change is not dramatic in 0.95 lagging power factor case. On the other hand, flexible power control shows the best performance maintaining stability and low curtailment over all the cases.

TABLE II: Total Curtailment

Dead Band / **PF Control**	**Fixed**			**Variable**
	$6\delta V$	$7\delta V$	$8\delta V$	$[6-8]\delta V$
PF = 1	0.149	0.128	0.074	0
PF = 0.95 (lagging)	0.380	0.261	0.244	0
PF = 0.95 (leading)	0.152	0.155	0.121	0.022
PF $\leq |0.95|$	0	0.009	0	0

B. Numerical Tests on IEEE 123-bus Feeder

Further computational tests have been carried out on the modified IEEE 123-bus feeder shown in Fig. 10 to test the scalability of the proposed dead band tuning method. The test network has 4 step voltage regulators, labeled from SVR-1 to SVR-4, which are placed with respect to different phasing configurations according to the original IEEE data sheet. The existing network has been assumed to have 23 PV generation sites, 6 of which are featured as utility-scale PV generation sites, each of which has a capacity of 500 kVA interconnected with the three-phase inverter units that can be managed by the utility. The rest of the PV sites are interconnected to the network through the single-phase inverter units rated as 5 kW of active power output rating without direct utility control.

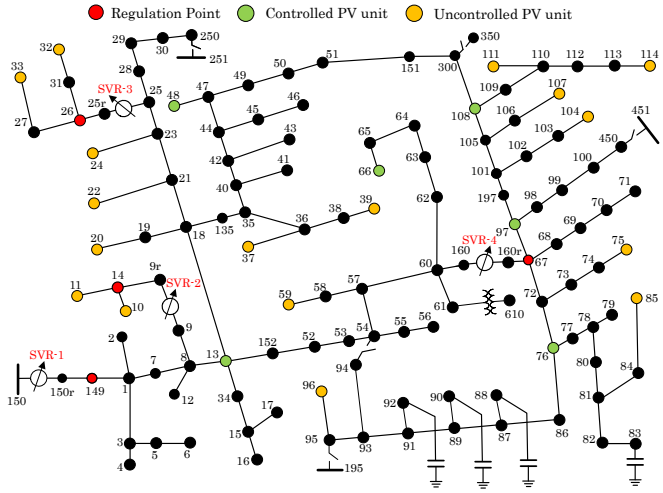

Fig. 10: The modified IEEE 123-bus test network.

The proposed optimization problem's solution space is larger for the IEEE 123-bus network due to the presence of multiple regulator equipment. Hence, the size of the solution space should be kept small enough to obtain a solution within a reasonable duration of time and optimality. In this network case, the optimization routine can be run for a daily operation with 1-hour resolution. A minimum bandwidth of $4\delta V$ has been found as the lowest feasible solution valid for the entire optimization horizon. Hence, further increments on the minimum bandwidth have been tested up to $6\delta V$. The objective coefficients in (6i) is selected as $c_1 = 1000$, $c_2 = 5$, $c_3 = 100$. It can be seen from Table III that the dead band tuning approach can maintain an average dead band very close to the tightest bandwidth of $4\delta V$ while less number of total tap change count is obtained compared to the solution with a fixed dead band of $4\delta V$.

TABLE III: Number of Total Tap Change

Dead Band / PF Control	Fixed			Variable	
	$4\delta V$	$5\delta V$	$6\delta V$	$[4-8]\delta V$	Avg. DB
PF = 1	4	3	0	3	4.02
PF = 0.95 (lagging)	24	9	3	9	4.14
PF = 0.95 (leading)	6	0	0	0	4.08
PF $\leq$ |0.95|	5	1	0	2	4.01

Similar to the IEEE 13-bus system case, lagging power factor control incurs the highest number of tap position changes while unity, leading, and flexible power factor control cases result in comparably less total tap count.

Table IV summarizes the total amount of curtailed energy from PV inverters. The proposed dead band tuning approach performs better than a fixed dead band.

TABLE IV: Total Curtailment

Dead Band / PF Control	Fixed			Variable
	$4\delta V$	$5\delta V$	$6\delta V$	$[4-8]\delta V$
PF = 1	0.0517	0.1394	0	0
PF = 0.95 (lagging)	0.0875	0.1691	0.1377	0.0032
PF = 0.95 (leading)	0.0811	0	0	0
PF $\leq$ |0.95|	0.0984	0.0274	0	0

V. Conclusion

OLTCs and SVRs are common voltage regulation devices in distribution networks. These equipment are basically auto-transformers typically controlled by local feedback controllers that command mechanical switches to alter the transformer turns ratio. A bang-bang type control rule with a dead band is generally adopted to automate the tap-changing process. Due to the large penetration levels in PV-rich distribution networks, frequent tap switching are likely to occur. This paper proposes a systematic model-based optimal dead band tuning approach to prevent excessive tap switching from occurring in OLTC and SVR controllers. The proposed method is formulated as a MILP-based DOPF considering the unbalanced operation conditions of typical distribution networks with multi-phase configurations. Extensive numerical tests have been carried out on the IEEE 13-bus and IEEE 123-bus test systems operating under high PV penetration. According to the numerical test results, the proposed tuning method can help utilities to reduce the number of tap switching by dynamically adjusting the dead band parameter of the equipment controller and the amount of curtailed energy from the PV units. Moreover, the approach can extend the economic use-life of the regulation equipment. Future work is to conduct standardized comprehensive performance assessment of the available optimization-based LTC dispatch and control strategies.

References

[1] W. H. Kersting, *Distribution system modeling and analysis*. CRC press, 2006.

[2] R. Seguin, J. Woyak, D. Costyk, J. Hambrick, and B. Mather, "High-penetration pv integration handbook for distribution engineers," *Tech. Report, National Renewable Energy Lab. (NREL), Golden, CO*, 2016.

[3] S. Weckx, C. Gonzalez, and J. Driesen, "Combined central and local active and reactive power control of pv inverters," *IEEE Transactions on Sustainable Energy*, vol. 5, no. 3, pp. 776–784, 2014.

[4] O. Ceylan, S. Paudyal, and I. Pisica, "Nodal sensitivity-based smart inverter control for voltage regulation in distribution feeder," *IEEE Journal of Photovoltaics*, vol. 11, no. 4, pp. 1105–1113, 2021.

[5] B. Palmintier, J. Giraldez, K. Gruchalla, P. Gotseff, A. Nagarajan, T. Harris, B. Bugbee, M. Baggu, J. Gantz, and E. Boardman, "Feeder voltage regulation with high-penetration pv using advanced inverters and a distribution management system: A duke energy case study," *Tech. Report, National Renewable Energy Lab. (NREL), Golden, CO*, 2016.

[6] Integrated volt/var control brochure - Eaton. [Online]. Available: https://www.eaton.com/content/dam/eaton/products/utility-and-grid-solutions/grid-automation-systems/volt-var-management/volt-var-management-software/integrated-volt-var-control-br910005en.pdf

[7] F. Hillier and G. J. Lieberman, *Introduction to operations research 11th Ed.* McGraw-Hill Education, 2021.

[8] J. A. Taylor, *Convex optimization of power systems*. Cambridge University Press, 2015.

[9] R. R. Jha, A. Inaolaji, B. D. Biswas, A. Suresh, A. Dubey, S. Paudyal, and S. Kamalasadan, "Distribution grid optimal power flow (d-opf): Modeling, analysis, and benchmarking," *IEEE Transactions on Power Systems*, pp. 1–14, 2022.

[10] A. Inaolaji, A. Savasci, S. Paudyal, and S. Kamalasadan, "Accuracy of phase-decoupled and phase-coupled distribution grid power flow models," in *2021 IEEE Power Energy Society Innovative Smart Grid Technologies Conference (ISGT)*, 2021, pp. 1–5.

[11] S. Paudyal, C. A. Canizares, and K. Bhattacharya, "Optimal operation of distribution feeders in smart grids," *IEEE Transactions on Industrial Electronics*, vol. 58, no. 10, pp. 4495–4503, 2011.

[12] B. A. Robbins, H. Zhu, and A. D. Domínguez-García, "Optimal tap setting of voltage regulation transformers in unbalanced distribution systems," *IEEE Transactions on Power Systems*, vol. 31, no. 1, pp. 256–267, 2016.

[13] S. R. Shukla, S. Paudyal, and M. R. Almassalkhi, "Efficient distribution system optimal power flow with discrete control of load tap changers," *IEEE Transactions on Power Systems*, vol. 34, no. 4, pp. 2970–2979, 2019.

[14] W. Wu, Z. Tian, and B. Zhang, "An exact linearization method for oltc of transformer in branch flow model," *IEEE Transactions on Power Systems*, vol. 32, no. 3, pp. 2475–2476, 2016.

[15] A. Savasci, A. Inaolaji, S. Paudyal, and S. Kamalasadan, "Efficient distribution grid optimal power flow with discrete control of legacy grid devices," in *2021 IEEE Power & Energy Society General Meeting (PESGM)*. IEEE, 2021, pp. 1–5.

[16] A. Savasci, A. Inaolaji, and S. Paudyal, "Two-stage volt-var optimization of distribution grids with smart inverters and legacy devices," *IEEE Transactions on Industry Applications*, vol. 58, no. 5, pp. 5711–5723, 2022.

[17] D. Ranamuka, A. P. Agalgaonkar, and K. M. Muttaqi, "Online voltage control in distribution systems with multiple voltage regulating devices," *IEEE Transactions on Sustainable Energy*, vol. 5, no. 2, pp. 617–628, 2014.

[18] T.-T. Ku, C.-H. Lin, C.-S. Chen, and C.-T. Hsu, "Coordination of transformer on-load tap changer and pv smart inverters for voltage control of distribution feeders," *IEEE Transactions on Industry Applications*, vol. 55, no. 1, pp. 256–264, 2019.

[19] J.-H. Choi and S.-I. Moon, "The dead band control of ltc transformer at distribution substation," *IEEE Transactions on Power Systems*, vol. 24, no. 1, pp. 319–326, 2009.

[20] A. Savasci, A. Inaolaji, and S. Paudyal, "Optimal coordination of on-load tap changers with local control rules," in *2022 IEEE Industry Applications Society Annual Meeting (IAS)*, 2022, pp. 1–9.

[21] K. M. Muttaqi, A. D. T. Le, M. Negnevitsky, and G. Ledwich, "A coordinated voltage control approach for coordination of oltc, voltage regulator, and dg to regulate voltage in a distribution feeder," *IEEE Transactions on Industry Applications*, vol. 51, no. 2, pp. 1239–1248, 2015.

[22] M. D. Sankur, R. Dobbe, E. Stewart, D. S. Callaway, and D. B. Arnold, "A linearized power flow model for optimization in unbalanced distribution systems," *arXiv preprint arXiv:1606.04492*, 2016.

[23] J. Faiz and B. Siahkolah, "Differences between conventional and electronic tap-changers and modifications of controller," *IEEE Transactions on Power Delivery*, vol. 21, no. 3, pp. 1342–1349, 2006.

[24] M. Hartung, E.-M. Baerthlein, and A. Panosyan, "Comparative study of tap changer control algorithms for distribution networks with high penetration of renewables," in *CIRED Workshop*, no. 0376, 2014, pp. 1–5.

[25] A. Savasci, A. Inaolaji, and S. Paudyal, "Distribution grid optimal power flow integrating volt-var droop of smart inverters," in *2021 IEEE Green Technologies Conference (GreenTech)*, 2021, pp. 54–61.

[26] R. A. Jabr, "Linear decision rules for control of reactive power by distributed photovoltaic generators," *IEEE Transactions on Power Systems*, vol. 33, no. 2, pp. 2165–2174, 2018.

[27] Basic considerations for the application of ltc transformers and associated controls. [Online]. Available: https://beckwithelectric.com/wp-content/uploads/docs/app-notes/Beckwith-App-Note-17.pdf

[28] K. P. Schneider, B. A. Mather, B. C. Pal, C.-W. Ten, G. J. Shirek, H. Zhu, J. C. Fuller, J. L. R. Pereira, L. F. Ochoa, L. R. de Araujo, R. C. Dugan, S. Matthias, S. Paudyal, T. E. McDermott, and W. Kersting, "Analytic considerations and design basis for the ieee distribution test feeders," *IEEE Transactions on Power Systems*, vol. 33, no. 3, pp. 3181–3188, 2018.

Alper Savasci (S'19, M'23) received the B.S. degree in electrical and electronics engineering from Erciyes University, Kayseri, Turkey, in 2012. He received the M.Sc. degree in electrical engineering from Michigan Technological University, Houghton, MI, USA, in 2018, and the Ph.D. degree from the Florida International University, Miami, FL, USA, in 2023. His current research interests are distribution system modeling and optimization.

Adedoyin Inaolaji (S'19) received a B.Eng. degree in Electrical and Electronics Engineering from Covenant University, Ota, Nigeria, in 2014, and an M.S. degree in Electrical Engineering from the Department of Electrical and Computer Engineering, Florida International University (FIU), Miami, FL, USA in 2022, where she is currently working toward the Ph.D. degree in Electrical Engineering. Her research interests include distribution grid modeling, analysis, and optimization techniques.

Sumit Paudyal (S'07, M'12) received the B.E. degree from Tribhuvan University, Nepal in 2003, the M.Sc. degree from the University of Saskatchewan, Saskatoon, Canada, in 2008, and the Ph.D. degree from the University of Waterloo, Waterloo, Canada, in 2012, all in electrical engineering. He was a faculty member at Michigan Technological University, Houghton, MI, USA from 2012 to 2019. Since 2019, he is an Associate Professor in the Department of Electrical and Computer Engineering at Florida International University, Miami, FL, USA. His research interests include distribution grid modeling, dynamic studies, and optimization techniques in power systems.